A comprehensive study of the COVID-19 impact on PM$_{2.5}$ levels over the contiguous United States: A deep learning approach

Masoud Ghahremanloo [a], Yannic Lops [a], Yunsoo Choi [a,*], Jia Jung [a], Seyedali Mousavinezhad [a], Davyda Hammond [b]
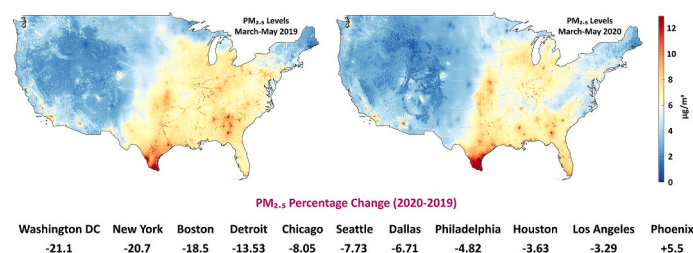
[a] Department of Earth and Atmospheric Sciences, University of Houston, Houston, TX, 77004, USA
[b] Oak Ridge Associated Universities, Oak Ridge, TN, 37830, USA

HIGHLIGHTS

- Deep learning was used to accurately estimate daily PM$_{2.5}$ levels at ground level.
- Greater decreases in human mobility resulted in more reductions in PM$_{2.5}$ levels.
- Washington DC experienced the highest PM$_{2.5}$ reduction compared to other regions.
- Phoenix was the only region with an increase in PM$_{2.5}$ levels in this study.
- Changes in levels of BC, OC, SO$_2$, SO$_4$, and NO$_2$ notably impacted PM$_{2.5}$ levels.

GRAPHICAL ABSTRACT

Washington DC	New York	Boston	Detroit	Chicago	Seattle	Dallas	Philadelphia	Houston	Los Angeles	Phoenix
-21.1	-20.7	-18.5	-13.53	-8.05	-7.73	-6.71	-4.82	-3.63	-3.29	+5.5

ARTICLE INFO

ABSTRACT

We investigate the impact of the COVID-19 outbreak on PM$_{2.5}$ levels in eleven urban environments across the United States: Washington DC, New York, Boston, Chicago, Los Angeles, Houston, Dallas, Philadelphia, Detroit, Phoenix, and Seattle. We estimate daily PM$_{2.5}$ levels over the contiguous U.S. in March–May 2019 and 2020, and leveraging a deep convolutional neural network, we find a correlation coefficient, an index of agreement, a mean absolute bias, and a root mean square error of 0.90 (0.90), 0.95 (0.95), 1.34 (1.24) μg/m^3, and 2.04 (1.87) μg/m^3, respectively. Results from Google Community Mobility Reports and estimated PM$_{2.5}$ concentrations show a greater reduction of PM$_{2.5}$ in regions with larger decreases in human mobility and those in which individuals remain in their residential areas longer. The relationship between vehicular PM$_{2.5}$ (i.e., the ratio of vehicular PM$_{2.5}$ to other sources of PM$_{2.5}$) emissions and PM$_{2.5}$ reductions ($R = 0.77$) in various regions indicates that regions with higher emissions of vehicular PM$_{2.5}$ generally experience greater decreases in PM$_{2.5}$. While most of the urban environments —— Washington DC, New York, Boston, Chicago, Los Angeles, Houston, Dallas, Philadelphia, Detroit, and Seattle —— show a decrease in PM$_{2.5}$ levels by 21.1%, 20.7%, 18.5%, 8.05%, 3.29%, 3.63%, 6.71%, 4.82%, 13.5%, and 7.73%, respectively, between March–May of 2020 and 2019, Phoenix shows a 5.5% increase during the same period. Similar to their PM$_{2.5}$ reductions, Washington DC, New York, and Boston, compared to other cities, exhibit the highest reductions in human mobility and the highest vehicular PM$_{2.5}$ emissions, highlighting the great impact of human activity on PM$_{2.5}$ changes in eleven regions. Moreover, compared to changes in meteorological factors, changes in pollutant concentrations, including those of black

carbon, organic carbon, SO$_2$, SO$_4$, and especially NO$_2$, appear to have had a significantly greater impact on PM$_{2.5}$ changes during the study period.

1. Introduction

On the last day of 2019, China reported the first cases of an abnormal lung infection in Wuhan to the World Health Organization (WHO) (Ghahremanloo et al., 2021a). On January 7, 2020, WHO announced the identification of a new virus, severe acute respiratory syndrome coronavirus 2 (SARS-CoV-2), and on January 30, 2020, a worldwide public health emergency was declared by WHO (WHO, 2020). In the United States, the first case was reported to the Centers for Disease Control and Prevention on January 20, 2020, and the U.S. president declared a public health emergency on January 31, 2020 (Aubrey, 2020; Robertson, 2020). The coronavirus disease 2019 (COVID-19) is an extremely infectious respiratory illness, especially in those who have been in close contact with already infected individuals (Bherwani et al., 2020; Cascella et al., 2021). Therefore, its rapid spread can be controlled by implementing suitable social distancing measures and avoiding crowded places such as public transport, stadiums, and even family gathering spots (Bherwani et al., 2020; Gautam, 2020). Since the outbreak of the COVID-19 pandemic, many countries around the world have implemented lockdown or stay-at-home advisory strategies to combat the spread of the virus (Ghahremanloo et al., 2021a), and half of the world population has experienced a degree of lockdown by the end of March 2020 (Tosepu et al., 2020). Despite these lockdowns, or stay-at-home advisory strategies, as of December 2021, more than 5.3 million deaths and 276 million confirmed cases of the COVID-19 globally have been reported (https://covid19.who.int/).

Lockdown situations, and the following decrease in human activity, have led to major reductions in pollution levels, providing researchers with a unique opportunity to investigate the impact of reduced human activity on air pollution levels. Human activity, directly or indirectly, is one of the main factors responsible for various types of pollutant emissions into the atmosphere. One of the major pollutants in the atmosphere is particulate matter with an aerodynamic diameter of less than 2.5 μm (PM$_{2.5}$) (Ghahremanloo et al., 2021b). Although mucociliary clearance eliminates the majority of the particulate matter we breathe, the PM$_{2.5}$ fraction can reside inside the lungs and penetrate the circulatory system (Ghahremanloo et al., 2021b). Because of the serious health effects of PM$_{2.5}$, such as respiratory disease (Polezer et al., 2018) and cardiovascular illness (Hayes et al., 2020), WHO has listed PM$_{2.5}$ as a major public health threat (Lancet, 2006). A number of studies have reported significant reductions in concentrations of PM$_{2.5}$ and other pollutants in various regions of the world, such as the United States (Chen et al., 2021; Pan et al., 2020; Zangari et al., 2020), China (Yin et al., 2021), East Asia (Ghahremanloo et al., 2021a), Europe (Baldasano, 2020; Tobías et al., 2020), and South America (Krecl et al., 2020) resulting from the COVID-19 lockdowns, or stay-at-home advisory strategies. For instance, Ghahremanloo et al. (2021a) used satellite images to examine the impact of COVID-19 on air pollution levels in the Beijing-Tianjin-Hebei (BTH) and Wuhan regions of China, and in Seoul, South Korea, and Tokyo, Japan. According to their results, column densities of NO$_2$, HCHO, SO$_2$, and CO in Wuhan, China decreased by 83%, 11%, 71%, and 4%, respectively, in February 2020 compared to those in February 2019. They also found a 62% decrease in aerosol optical depth (AOD) levels during the same period in Wuhan. Lal et al. (2020) also reported a substantial global decrease in the AOD (0.1–0.2) and the column densities of CO ($<1.81 \times 10^{18}$ molecules cm^{-2}) and NO$_2$ (1.2×10^{15} molecules cm^{-2}) during February–March 2020 compared to those on similar days in 2019. By comparing surface concentrations of pollutants before and during the lockdown in Salé, Morocco, Otmani et al. (2020) found a major decrease in concentrations of PM$_{10}$ (75%), SO$_2$ (49%), and NO$_2$ (96%). Moreover, COVID-19 lockdowns, or stay-at-home advisory

policies resulted in PM$_{2.5}$ reductions of almost 30% in central China (Xu et al., 2020), 5.9% in northern China (Bao and Zhang, 2020), and 35–39% in several cities in India (Chauhan and Singh, 2020; Mahato et al., 2020; Parida et al., 2021). Rodríguez-Urrego and Rodríguez-Urrego (2020) investigated 50 capital cities across the globe and reported both increased and decreased PM$_{2.5}$ levels during the COVID-19 outbreak. According to their results, several capital cities such as Tokyo (Japan), Paris (France), London (Britain), Vienna (Austria), and Jakarta (Indonesia) experienced an increase in PM$_{2.5}$ concentrations, while other cities such as Delhi (India), Dhaka (Bangladesh), Tehran (Iran), Bogota (Colombia), and Mexico City (Mexico) reported reductions. Since most of the PM$_{2.5}$ ingredients are short-lived pollutants, it is also worth conducting similar studies to investigate the impact of the COVID-19 lockdowns on air pollution levels in receipt regions like the Arctic. Previous studies have shown a positive impact of the COVID-19 lockdown on other pollutants such as ozone (Bouarar et al., 2021; Khan et al., 2021; Tahir and Batool, 2020) in Arctic regions.

Several studies, most of which have used either surface measurements or satellite images for their analysis, have examined the impact of the COVID-19 pandemic on air pollution levels. Although their pollutant surface observations at ground stations have been precise, they took place at a limited number of ground stations over the United States and globally. Thus, because of the limited spatial coverage of the ground stations, studies have not been able to determine precise surface pollution levels, especially those in urban and suburban regions, with significant changes in the spatial distribution of pollutants (Ghahremanloo et al., 2021b). In addition, satellite instruments that measure the column densities of pollutants are seriously limited at capturing surface concentrations of pollutants, required in public health studies. The high frequency of missing values in satellite images results in data loss, restricting high-quality analyses of pollution reductions resulting from reduced human activity (Lops et al., 2021). Such limitations further highlight an essential need to develop advanced models that capture the spatiotemporal distribution of pollutants at high resolutions, particularly in regions with limited or no surface measurements, to improve the accuracy of analyses regarding the impact of COVID-19 on air pollution levels. Numerous studies have leveraged machine learning (ML) and deep learning (DL) to capture the spatiotemporal distribution of pollution levels (de Hoogh et al., 2019; Eslami et al., 2020; Ghahremanloo et al., 2021b, 2021c; Hu et al., 2017; Lops et al., 2020; Park et al., 2020; Sayeed et al., 2020; Yeo et al., 2021). Ghahremanloo et al. (2021b) used random forest (RF) to achieve a correlation coefficient (R) and a mean absolute bias (MAB) of 0.83–0.90 and 1.47–1.77 μg/m^3, respectively, in high-resolution PM$_{2.5}$ estimation. Hu et al. (2017) also used RF to incorporate various predictor variables such as satellite AOD and meteorological factors to estimate PM$_{2.5}$ levels over the contiguous United States (CONUS) in 2011. Their model also showed high accuracy ($R = 0.89$) of surface PM$_{2.5}$ estimation over the CONUS. Moreover, Ghahremanloo et al. (2021c) leveraged a deep convolutional neural network (Deep-CNN) to estimate the spatiotemporal distribution of surface NO$_2$ levels at high resolution. Their results revealed the promising performance of Deep-CNN at capturing surface NO$_2$ levels, with an R and an MAB of 0.91 and 1.75 ppb, respectively.

This study presents a DL approach to investigating the impact of COVID-19 lockdowns, or stay-at-home advisory strategies on changes in PM$_{2.5}$ concentrations in eleven metropolitan areas over the CONUS. As mentioned before, previous studies mainly used either ground stations or satellite images to examine changes in air pollution during the COVID-19 pandemic. However, when monitoring PM$_{2.5}$ changes over large urban environments, both approaches have serious limitations, discussed in the previous paragraph. Therefore, this study leverages

Deep-CNN to produce accurate daily PM$_{2.5}$ maps at a 5-km spatial resolution over the CONUS to study changes in PM$_{2.5}$ levels from March to May 2020, compared to similar days in 2019. The output of daily PM$_{2.5}$ grids over the CONUS do not contain missing values to improve the quality of analyses. Moreover, we use Google Community Mobility Reports to study people's mobility changes during the study period. We believe that this study is the first to comprehensively investigate PM$_{2.5}$ changes resulting from shutdowns and stay-at-home strategies during the COVID-19 outbreak in several metropolitan areas over the CONUS.

2. Study area and data

2.1. The contiguous United States (CONUS)

We analyze daily changes in PM$_{2.5}$ concentrations in eleven urban environments over the CONUS (Fig. 1) from March 1 to May 31, 2020, compared to similar days in 2019. We have selected eleven urban environments —— Washington DC, New York, Boston, Chicago, Los Angeles, Houston, Dallas, Philadelphia, Detroit, Phoenix, and Seattle —— based on their economic importance, pollution levels, populations, and areas. For the analyses, we have defined eleven boundaries around each urban environment to include all metropolitan areas, including downtown and suburban regions. Table 1 shows the latitude and longitude coordinates of the boundaries around the urban environments analyzed in this study, along with the exact dates of the lockdowns, or stay-at-home orders issued by each city (Wu et al., 2020). This table also displays the counties inside each region. Of note, the boundaries around three urban environments (Washington DC, New York, and Philadelphia) include more than one state. Therefore, the information of all included states appears in Table 1.

2.2. Datasets

In order to use Deep-CNN to estimate daily PM$_{2.5}$ concentrations over the CONUS from March to May 2019 and 2020, we have incorporated several predictor variables, including the weighted average PM$_{2.5}$ layer (WAPM), the weighted average NO$_2$ layer (WANO$_2$), model data from the Community Multiscale Air Quality (CMAQ) modeling system, meteorological factors, reanalysis data, land-use parameters, and the vegetation index. All the predictor variables are prepared over the CONUS during March–May 2019 and 2020. To train the Deep-CNN model, we use surface PM$_{2.5}$ observations as the target variable, including 63,303 samples in 2019 and 62,181 in 2020. More

Table 1

List of urban environments analyzed in this study. The Lat. and Long. columns refer to the latitude and longitude coordinates of the edges of the boundaries around each region. The fourth column lists the multiple counties inside each region, and the last column lists the effective dates of the stay-at-home/lockdown orders issued in each state.

| Region	Lat. (°N)	Long. (°W)	Counties Included	Effective Dates
Washington DC	38.60 to 39.60	77.30 to 76.10	DC, Baltimore, Arlington, Alexandria, Prince George's, Howard, Anne Arundel	Apr. 1 - May 15 - DC Mar. 30 - May 7 - MD
New York	40.30 to 41.10	74.60 to 73.30	New York, Kings, Queens, Bronx, Hudson, Richmond, Essex, Nassau, Union, Bergen	Mar. 22 - May 15 - NY Mar. 24 - May 2 - NJ
Philadelphia	39.80 to 40.20	75.40 to 74.75	Philadelphia, Delaware, Camden, Montgomery, Bucks, Burlington	Apr. 1 - May 8 - PA Mar. 24 - May 2 - NJ
Dallas	32.40 to 33.25	97.60 to 96.30	Dallas, Tarrant, Denton, Collin, Rockwall, Kaufman	Apr. 2 - Apr. 30 - TX
Los Angeles	33.40 to 34.60	119.0 to 117.0	Los Angeles, Orange, Riverside, Ventura	Mar. 19 - May 8 - CA
Chicago	41.45 to 42.50	88.20 to 87.25	Cook, DuPage, Lake, Will	Mar. 21 - Apr. 30 - IL
Boston	42.20 to 42.54	71.30 to 70.80	Suffolk, Norfolk, Middlesex	Mar. 24 - May 4 - MA
Houston	29.35 to 30.20	96.0 to 94.75	Harris, Fort Bend, Galveston	Apr. 2 - Apr. 30 - TX
Detroit	41.90 to 42.75	83.60 to 82.60	Wayne, Oakland, Macomb	Mar. 24 - May 15 - MI
Phoenix	33.17 to 33.98	112.5 to 111.5	Maricopa, Pinal	Mar. 31 - Apr. 30 - AZ
Seattle	47.12 to 48.06	122.6 to 122.0	King, Snohomish	Mar. 23 - May. 4 - WA
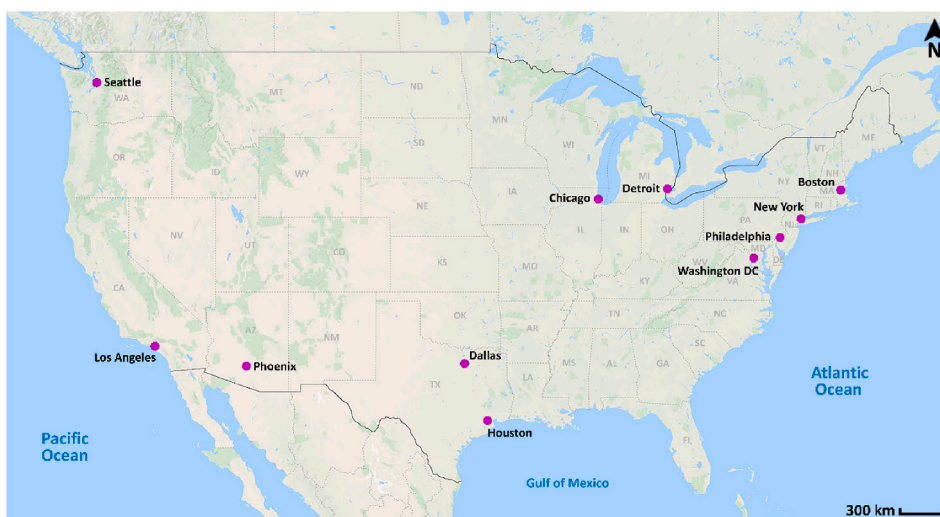
Fig. 1. Map of the CONUS (study areas). Pink dots represent the location of the eleven urban environments analyzed in this study. (For interpretation of the references to colour in this figure legend, the reader is referred to the Web version of this article.)

information about the datasets used in this study is available in the supplementary document.

3. Methodology

3.1. Deep convolutional neural network (Deep-CNN)

To estimate surface $PM_{2.5}$ concentrations over the CONUS from March to May 2019 and 2020, we trained one Deep-CNN model for each year. Both models consisted of seven layers, including one input layer, two convolutional layers, three fully-connected layers, and an output layer. We also added a dropout layer between the two convolutional layers to help reduce the overfitting issue (Ghahremanloo et al., 2021c). After feature engineering and finding the best combination of parameters, we retained only eleven predictor variables — WAPM, WANO$_2$, CMAQ PM$_{2.5}$, CMAQ HCHO, MERRA SO$_2$, MERRA BC, RD, PUS, PD, surface elevation, and SLH —— for the PM$_{2.5}$ estimation.

3.2. Feature selection

Several studies have addressed the negative impact of multi-collinearity on model performance (Kroll and Song, 2013; Wei et al., 2019). Therefore, it is crucial to properly remove predictor variables that are highly correlated with others. To find and exclude predictor variables with a high degree of multicollinearity, this study applied the variance inflation factor (VIF) (Ghahremanloo et al., 2021c; Kline, 2015; Wei et al., 2019). Previous studies (Cenfetelli and Bassellier, 2009; Ghahremanloo et al., 2021c; Kline, 2015; Kock and Lynn, 2012) have suggested various values as a VIF threshold, indicating multicollinearity among predictor variables. Following Kline (2015), to apply the VIF test on predictor variables, we set a VIF threshold equal to 5. Table S1 shows the results of the VIF test, which excluded two predictor variables (air temperature and surface pressure) from the data. After excluding parameters with large multicollinearity, we leveraged SHapley Additive exPlanations (SHAP) (Lundberg and Lee, 2017; SHAP, 2019) to find the best combination of predictor variables for surface PM$_{2.5}$ estimation. To this end, we removed less important parameters based on the SHAP feature importance scores of all the chosen parameters in the pre-trained models (Ghahremanloo et al., 2021c; Liu et al., 2020). SHAP calculates the importance of a feature by estimating PM$_{2.5}$ levels with and without the feature (Lundberg and Lee, 2017) and also leads to the interpretation of the output of black-box models such as the Deep-CNN (Ghahremanloo et al., 2021c; García and Aznarte, 2020). Among the available SHAP-based explanation methods, the *Deep SHAP* is used in this study because it performs better with DL models (Lundberg and Lee, 2017; SHAP, 2019).

3.3. Model evaluation

To validate the accuracy of the Deep-CNN at surface PM$_{2.5}$ estimation, we use the ten-fold cross-validation (10-CV) approach, which splits samples into ten non-overlapping groups, trains the model with nine groups, and tests the accuracy of PM$_{2.5}$ estimation with the remaining group (Ghahremanloo et al., 2021b, 2021c). This process is repeated until all ten groups are selected as test data. To evaluate the accuracy of the Deep-CNN, we use the correlation coefficient (*R*), the index of agreement (IOA), the mean absolute bias (MAB), and the root mean square error (RMSE) at every cycle, and the 10-cycle mean of each metric shows the final performance of the model (Ghahremanloo et al., 2021c). We also used spatial cross-validation (spatial-CV) to evaluate the spatial accuracy of the Deep-CNN, especially in areas with a small number of monitoring stations. The only difference between 10-CV and spatial-CV is that spatial-CV splits samples according to the ground stations while 10-CV splits samples randomly over all stations.

3.4. Google Community Mobility Reports

Google Community Mobility Reports (https://www.google.com/covid19/mobility/) release information about temporal mobility trends across regions for various types of places such as grocery stores and pharmacies, parks, transit stations, workplaces, and residential areas. The baseline day for each region is the median value from the five-week period from January 3 to February 6, 2020, in that region. It should be noted that the baseline is not a single value but consist of seven individual baseline values for each day in each category. Therefore, the same number of visitors on two different days could result in various percentage changes. The category "Parks" refers to places such as public gardens, castles, national forests, campgrounds, and observations decks, and the category "Transit Stations" represents places such as subway stations, seaports, taxi stands, highway rest stops, and car rental agencies. Although all categories measure changes in the total number of visitors, the "Residential" category shows only changes in duration. According to Google, "These reports are created with aggregated, anonymized sets of data from users who have turned on the location history setting, which is off by default." It should be noted that the Google Community Mobility Reports are not based on quality-assured data sources. Therefore, these data should be used with caution.

4. Results and discussion

4.1. Validation of the resampled CMAQ and NLDAS datasets

Figs. S1 and S2 represent the validation results of the original and resampled CMAQ datasets in 2019 and 2020, respectively, showing moderate accuracy of CMAQ at estimating daily surface concentrations of PM$_{2.5}$ and HCHO over the CONUS. Figs. S3–S6 also display validation results of NLDAS meteorological factors against surface observations in 2019 and 2020. Results show the very high capability of NLDAS at modeling various meteorological factors, including surface pressure, air temperature, specific humidity, and LRad over the study area. Previous studies (Ghahremanloo et al., 2021c; Luo et al., 2003) have also confirmed the high accuracy of NLDAS meteorological factors over the CONUS. The accuracy of NLDAS wind speed (*R*-2019 = 0.58 and *R*-2020 = 0.54) and SRad (*R*-2019 = 0.69 and *R*-2020 = 0.81), however, was lower than that of the other variables. The figures also reveal that cubic convolution interpolation, used to resample CMAQ and NLDAS datasets, slightly improved the accuracy of several parameters, especially with regard to the MAB. For instance, this approach decreased the MAB of surface pressure in 2019 from 3.69 mbars (mb) to 3.46 mb. The resampling approach also improved the accuracy of the other variables —— LRad, SRad, air temperature, and CMAQ PM$_{2.5}$ —— in 2019 and 2020.

Table 2

Results of the ten-fold cross-validation (10-CV) and spatial cross-validation (spatial-CV), which show the performance of two Deep-CNN models at estimating surface PM$_{2.5}$ levels in 2019 and 2020. The evaluation metrics include the correlation coefficient (*R*), the index of agreement (IOA), the mean absolute bias (MAB), and the root mean square error (RMSE). The MAB and RMSE are in µg/m^3, and % refers to the error (i.e., MAB or RMSE) value divided by mean observed PM$_{2.5}$.

Year	10-CV				Spatial-CV			
	R	IOA	MAB (%)	RMSE (%)	*R*	IOA	MAB (%)	RMSE (%)
2019	0.90	0.95	1.34 (19)	2.04 (29)	0.83	0.91	1.73 (25)	2.63 (37)
2020	0.90	0.95	1.24 (19)	1.87 (28)	0.84	0.91	1.66 (25)	2.47 (37)

4.2. Model evaluation

Table 2 shows the validation results of the Deep-CNN at estimating daily concentrations of surface $PM_{2.5}$ from March to May 2019 and 2020 over the CONUS. With an R, IOA, MAB, and RMSE of 0.90 (0.90), 0.95 (0.95), 1.34 (1.24) μg/m³, and 2.04 (1.87) μg/m³, respectively, the Deep-CNN shows promising performance at surface $PM_{2.5}$ estimation in 2019 (2020). A number of studies have estimated surface $PM_{2.5}$ levels in the CONUS. Using a two-stage spatial statistical model, Hu et al. (2014) obtained an R of 0.82 in an estimation of surface $PM_{2.5}$ in the southeastern United States. Lee et al. (2016) also leveraged a mixed-effects model to achieve a relatively high accuracy (R = 0.74–0.85) at estimating $PM_{2.5}$ levels in California from 2006 to 2012. Ghahremanloo et al. (2021b) used RF to estimate surface $PM_{2.5}$ levels over Texas from 2014 to 2018 and found an R ranging from 0.83 to 0.90 and an MAB ranging from 1.47 to 1.77 μg/m³. The results of spatial-CV, listed in Table 2, also show the spatial performance of the Deep-CNN at estimating surface $PM_{2.5}$ levels in 2019 (2020) with an R, IOA, MAB, and RMSE of 0.83 (0.84), 0.91 (0.91), 1.73 (1.66) μg/m³, and 2.63 (2.47) μg/m³, respectively. Since the model is validated against stations it has not been trained with, however, the spatial-CV accuracy of Deep-CNN is lower than that determined by 10-CV. This finding is in agreement with the findings of previous studies (Ghahremanloo et al., 2021c; Li et al., 2017; Park et al., 2020). In Fig. 2, estimated $PM_{2.5}$ is compared to corresponding $PM_{2.5}$ observations, further highlighting the strong capacity of Deep-CNN to estimate surface $PM_{2.5}$ concentrations.

Fig. 3 displays the spatial distribution of the estimated $PM_{2.5}$ concentrations at a 5-km spatial resolution over the CONUS from March to May 2019 and 2020. The estimated $PM_{2.5}$ levels are higher in the eastern CONUS than in the western regions, particularly over urban environments such as Phoenix, Houston, and Los Angeles. This finding is consistent with the findings of previous studies (Di et al., 2016; Hu et al., 2017; Park et al., 2020) that estimated $PM_{2.5}$ over the CONUS. Moreover, Fig. 3 shows that the Deep-CNN successfully captures $PM_{2.5}$ concentrations on most highways over the CONUS. Fig. 3 also plots the mean $PM_{2.5}$ concentrations at ground stations over the estimated $PM_{2.5}$ maps from March to May 2019 and 2020 to show the performance of the Deep-CNN in $PM_{2.5}$ estimation. Results reveal that estimated and observed $PM_{2.5}$ concentrations exhibit a similar pattern over the study area, indicating the promising capability and accuracy of the Deep-CNN at estimating the spatiotemporal distribution of $PM_{2.5}$ levels over the CONUS.

Fig. 3 reveals relatively high $PM_{2.5}$ concentrations in southern Texas in 2019 and 2020. In 1994, the governments of the United States, Mexico, and Canada signed the North American Free Trade Agreement (NAFTA) (Text - H.R.3450 - 103rd Congress) to create a free trade zone. Since that time, NAFTA has fostered the growth and accumulation of industrial regions and rapid population growth in regions close to the U. S.-Mexico border (Karnae and John, 2019). In light of these changes, the U.S. EPA predicted that air pollution would be a significant problem in regions close to the border (Karnae and John, 2019). Chow et al. (2000) also investigated the cross-boundary transport of air pollution across the U.S.-Mexico border, concluding that the pollution levels transported from Mexico to the U.S. were three times as high as those flowing in the opposite direction. Several studies have investigated the impact of long- and short-range transport on air pollution levels in various regions of the world (Jaffe et al., 2004; Liang et al., 2004; Pouyaei et al., 2020). There are various sources impacting $PM_{2.5}$ levels in southern Texas. Karnae and John (2019) used positive matrix factorization (PMF) to investigate the percentage contributions of various aerosols influencing $PM_{2.5}$ levels in southern Texas. According to their study, secondary sulfate, mainly from southern, southwestern, and southeastern regions, is the dominant aerosol contributing to $PM_{2.5}$ concentrations in this region. Another major contributor is sea salt sulfates from the Gulf of Mexico (southeast) and the hypersaline Laguna Madre (south-southwest) in Mexico (Karnae and John, 2019). The transport of pollutants to coastal regions increases acid formation (Karnae and John, 2019). Although sea salt is mainly composed of sodium chloride (NaCl), elevated acidity results in dechlorination or dehalogenation, in which the Cl^- in sea salt is replaced by sulfate and nitrate, producing sea salt sulfate (Hasheminassab et al., 2014). The third major contributor is fresh marine aerosols from the Gulf of Mexico, elevating $PM_{2.5}$ levels in southern Texas (Karnae and John, 2019).

Fig. S7 presents the importance of the features used in $PM_{2.5}$ estimation and describes the influence of each predictor variable on the model output (i.e., estimated surface $PM_{2.5}$ concentrations). The most important variable in the model is the WAPM. This finding is in agreement with the findings of previous studies (Hu et al., 2017; Park et al., 2020). The remaining important features are the RD, PUS, PD, surface elevation, SLH, CMAQ $PM_{2.5}$, CMAQ HCHO, $WANO_2$, MERRA SO_2, and MERRA BC. In Fig. S7a in the supplement, red designates the highest value of the feature while blue represents the lowest. The high (low) SHAP value of a feature means that the feature increases (decreases) the output (i.e., estimated $PM_{2.5}$ levels) value (Ghahremanloo et al., 2021c). According to Fig. S7a, the WAPM, RD, PUS, PD, CMAQ $PM_{2.5}$, CMAQ HCHO, $WANO_2$, MERRA SO_2, and MERRA BC positively impact the output (i.e., estimated $PM_{2.5}$ levels) of the Deep-CNN model, although a degree of mixed impact (i.e., positive and negative) occurs in some
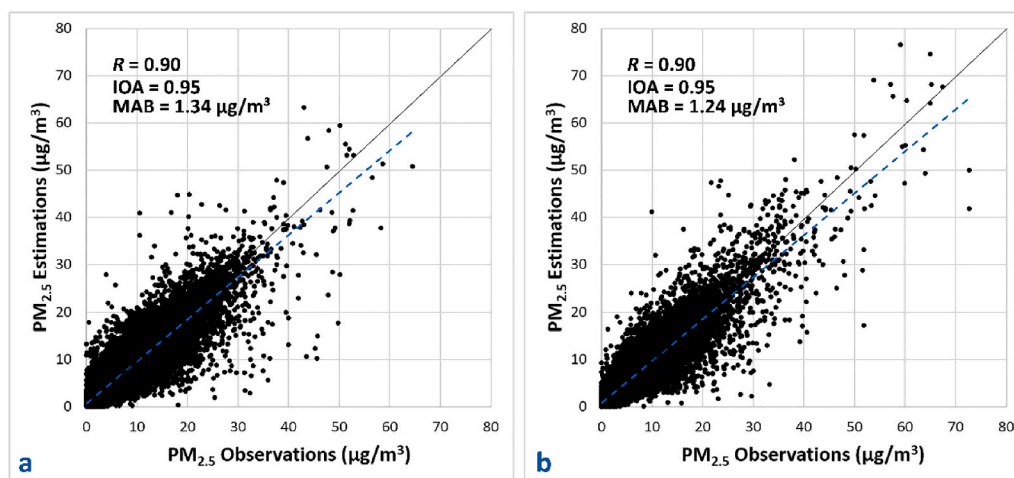

Fig. 2. Scatterplots of the ten-fold cross-validation (10-CV) results showing the performance of the deep convolutional neural network (Deep-CNN) at estimating surface concentrations of $PM_{2.5}$ over the CONUS from March to May 2019 (a) and 2020 (b). The R, IOA, and the MAB refer to the correlation coefficient, index of agreement, and the mean absolute bias, respectively.
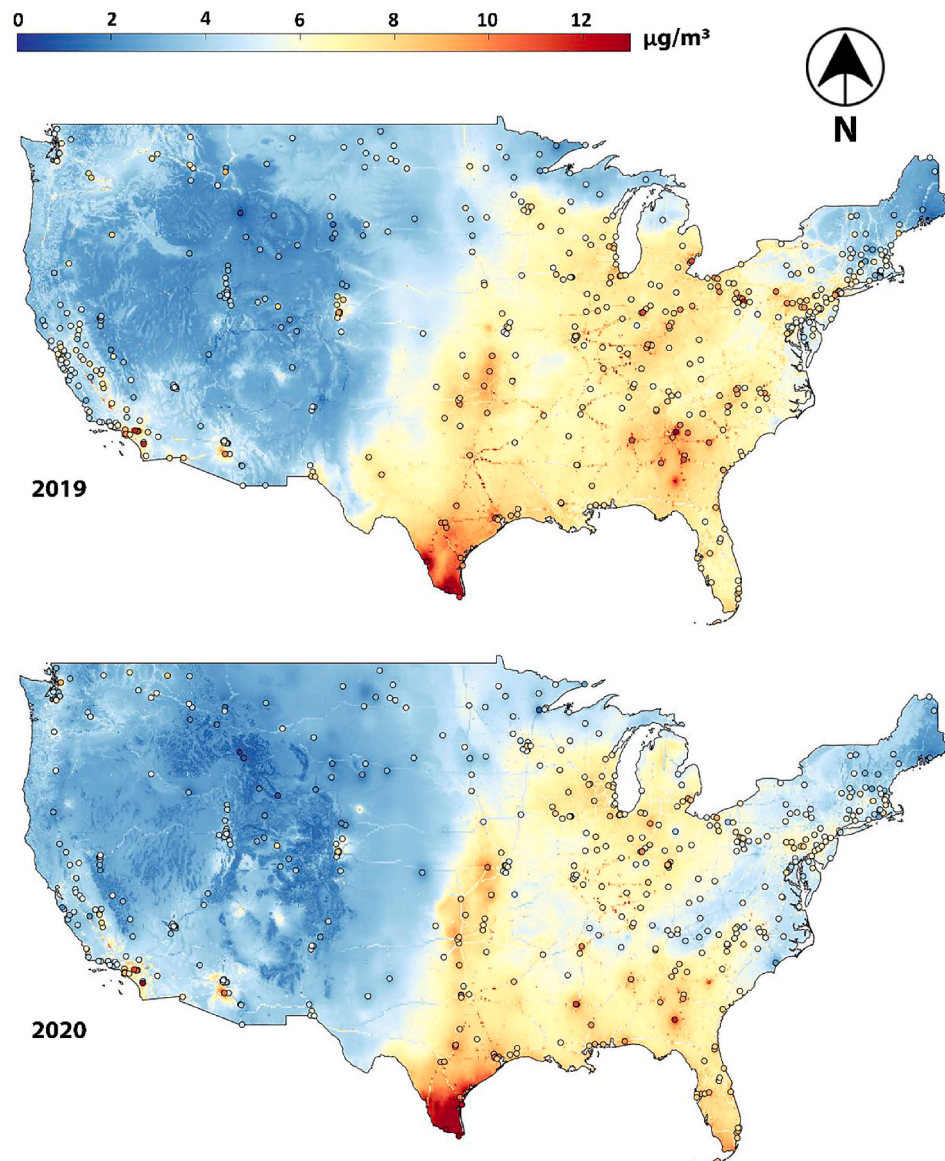
Fig. 3. The spatial distribution of mean estimated PM$_{2.5}$ levels over the CONUS from March to May 2019 (top) and 2020 (bottom). The circles show the mean observed PM$_{2.5}$ concentrations from the EPA stations during the study period, and the background maps represent the estimated PM$_{2.5}$ levels using deep learning (DL).

Table 3
Percentage changes in human mobility to various types of places, including grocery-pharmacy, workplaces, transit stations, and parks in the eleven study regions between March–May of 2020 and the baseline (median value from the five-week period ranging from January 3 to February 6, 2020). The column "Residential" refers to percentage changes in the amount of time people stayed in their residential areas compared to the baseline. The column "PM$_{2.5}$ Change" also shows the percentage changes in the mean PM$_{2.5}$ levels between March–May of 2020 and 2019. All numbers represent percentages.

Region	PM$_{2.5}$ Change	Grocery-Pharmacy	Workplace	Residential	Transit Stations	Parks
Washington DC	−21.1	−14.40	−43.69	18.44	−47.28	16.53
New York	−20.7	−14.57	−47.19	20.34	−53.35	−3.64
Boston	−18.5	−16.25	−47.63	20.43	−57.38	13.14
Detroit	−13.53	−11.35	−44.72	17.26	−32.22	63.68
Chicago	−8.05	−3.51	−37.21	15.09	−31.79	19.32
Seattle	−7.73	−11.33	−45.46	17.86	−44.98	26.78
Dallas	−6.71	−4.36	−36.48	14.64	−24.67	14
Philadelphia	−4.82	−11.09	−39.75	15.76	−44.45	11.94
Houston	−3.63	−1.49	−34.37	14.26	−13.09	9.17
Los Angeles	−3.29	−10.39	−37.33	17.14	−41.66	−23.56
Phoenix	5.5	−7.00	−34.13	12.32	−31.16	−11.15

features such as the PUS. The RD, PUS, and PD refer to vehicles and human activity, major sources of pollutants such as NO_2 and SO_2 (Ghahremanloo et al., 2021a), both of which are the precursors of nitrate and sulfate, respectively, two of the main ingredients of $PM_{2.5}$ (Ghahremanloo et al., 2021b). The only variable negatively impacting the model output is surface elevation. Generally, less human activity takes place at higher altitudes with stronger winds, providing conditions favorable to pollution dispersion (Ghahremanloo et al., 2021b; Hu et al., 2014). As all three gases — HCHO, NO_2, and SO_2 — are precursors of $PM_{2.5}$ (Huang et al., 2022), they positively impact estimates of $PM_{2.5}$ concentrations. As BC is another main component of $PM_{2.5}$ (Targino et al., 2016; Viidanoja et al., 2002), higher BC usually results in elevated $PM_{2.5}$ levels.

4.3. Reduction in mobility and its impact on $PM_{2.5}$ levels

Table 3 represents the percentage changes in human mobility to the various categories of places, including grocery stores and pharmacies, workplaces, residential areas, transit stations, and parks in the eleven regions from March to May 2020, compared to the baseline (median value from January 3 to February 6, 2020). This table also lists the percentage changes in the mean estimated $PM_{2.5}$ concentrations over the eleven urban environments in March–May 2020, compared to similar days in 2019. Although the baseline for the mobility changes is not March to May 2019, the mobility change data can still represent the amount of changes in human activity and contribute to the interpretation of $PM_{2.5}$ changes. According to Table 3, three urban environments (Washington DC, New York, and Boston) experienced the highest reductions in mean $PM_{2.5}$ levels (i.e., −21.1%, −20.7%, and −18.5%, respectively) in 2020, compared to those in 2019. Accordingly, these regions had the highest percentage reductions in the number of visitors to grocery stores-pharmacies, workplaces, and transit stations. The highest percentage increases in the amount of time people stayed in their residential areas also occurred in Washington DC (18.44%), New York (20.34%), and Boston (20.43%), further highlighting the impact of mobility changes and stay-at-home policies on $PM_{2.5}$ changes.

In addition, Table 3 displays a 5.5% increase in the mean $PM_{2.5}$ concentrations in Phoenix between March–May of 2020 and 2019. In fact, Phoenix, compared to other regions, also experienced the lowest percentage reduction in the number of individuals who went to their workplaces (−34.13%) and the lowest percentage increase (12.32%) in the amount of time people stayed in residential areas. Phoenix also had one of the lowest percentage reductions in the number of visitors to other places, including grocery stores and pharmacies (−7%) and transit stations (−31.16%). These findings indicate that human activity in Phoenix did not decline as much as it did in other urban environments. The correlation coefficient between $PM_{2.5}$ percentage changes in all regions and corresponding percentage changes in the "Grocery-Pharmacy", "Workplace", "Residential", "Transit Stations", and "Parks" categories were 0.67, 0.83, −0.87, 0.61, and −0.34, respectively. These findings indicate that the longer people stayed in their residential areas and the more they avoided visiting grocery stores, pharmacies, workplaces, and transit stations, the more significant the $PM_{2.5}$ reduction was in the area; however, the relatively small negative correlation between the percentage changes in $PM_{2.5}$ and the percentage changes in the "Parks" category appears to be inconsistent, calling for further research in this regard. Fig. S8 shows a decrease followed by an increase in the percentage change of human mobility to parks in almost all regions. The increase in park visitation can be attributed to the people's desire to visit parks and partake in other recreational activities when lockdown mandates were gradually being eased. Studies have found evidence of both the negative impact of lockdowns on mental health across several social groups and globally (Adams-Prassl et al., 2020; Banks and Xu, 2020; Elmer et al., 2020; Rossi et al., 2020) and the positive impact of access to public green spaces and parks on mental wellbeing and physical activity (Bedimo-Rung et al., 2005; Wood et al., 2017).

Another possible factor for the increase in the number of people visiting parks is the seasonal transition from winter to spring. The negative correlation between percentage changes in $PM_{2.5}$ levels in all regions and the corresponding percentage changes in the "Parks" category indicates that as more people avoided visiting parks, $PM_{2.5}$ levels tended to increase. As the Google mobility report does not specify the mode of transport (e.g., vehicular or walking) people used to visit parks, studies could analyze the mode of transportation that people tended to use to visit green and recreational spaces as the lockdowns were gradually eased.

Fig. S8 also displays the daily percentage changes in human mobility to the various types of places in the eleven regions between March–June of 2020 and the baseline days. According to the figure, human mobility in all regions began to decrease during the first days of March 2020, with the highest percentage reductions occurring in the number of visitors to workplaces (a 40.7% mean reduction) and transit stations (a 38.4% mean reduction). Visits to grocery stores/pharmacies peaked before the sudden decrease during the first half of March in all regions, which can be attributed to people flocking to grocery stores and pharmacies in need of items.

The relationship between $PM_{2.5}$ percentage changes in March–May 2020 compared to 2019 and vehicular $PM_{2.5}$ (i.e., the ratio of vehicular $PM_{2.5}$ to other sources of $PM_{2.5}$) in the eleven urban environments over the CONUS is shown in Fig. 4. As mentioned in Section 2.2.8, we were using the 2017 NEI to calculate vehicular $PM_{2.5}$. The figure shows a significant correlation ($R = -0.77$) between $PM_{2.5}$ percentage changes and vehicular $PM_{2.5}$, indicating that regions with more vehicular $PM_{2.5}$ experienced greater $PM_{2.5}$ reductions in 2020 compared to 2019. For instance, $PM_{2.5}$ levels in Washington DC decreased 21.1% in March–May 2020 compared to 2019, and 8.82% of the total $PM_{2.5}$ emissions in this region were attributed to vehicle use; however, in Phoenix, with a 5.5% increase in $PM_{2.5}$ levels, only 4.15% of $PM_{2.5}$ emissions were from vehicles. Fig. 4 also shows the upper and lower limits of the 95% confidence interval (CI) for the linear regression line of the population. Since we use a small sample size (i.e., eleven urban environments) from the population, the 95% CI shows the area in which, with 95% probability,
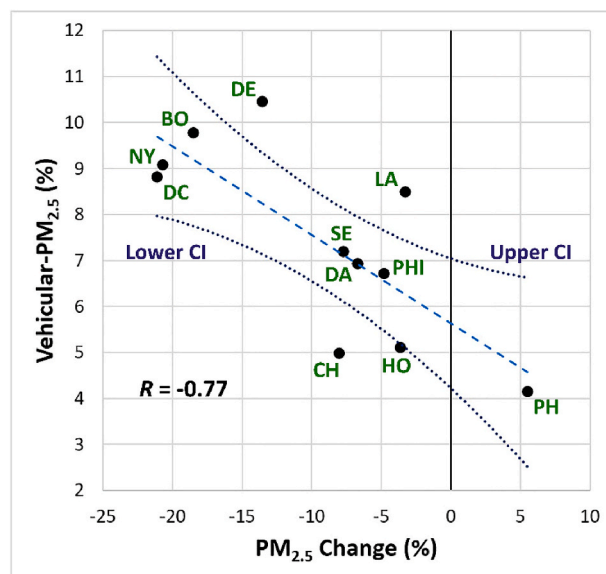
Fig. 4. Scatterplot showing the relationship between percentage changes of $PM_{2.5}$ between March–May of 2020 and 2019 and vehicular $PM_{2.5}$ (i.e., the ratio of vehicular $PM_{2.5}$ to other sources of $PM_{2.5}$) in the eleven urban environments over the CONUS, including Washington DC (DC), New York (NY), Boston (BO), Chicago (CH), Los Angeles (LA), Houston (HO), Philadelphia (PHI), Detroit (DE), Phoenix (PH), Dallas (DA), and Seattle (SE). The Upper CI and Lower CI refer to the upper and lower limits of the 95% confidence interval, respectively.

Table 4

Percentage (%) and absolute (Diff.) changes in parameters, including air temperature (T), specific humidity (Hum), surface pressure (Pres), the planetary boundary layer height (PBLH), and surface concentrations of dust, sea salt (Salt), black carbon (BC), organic carbon (OC), SO_2, SO_4, and NO_2 in the eleven urban environments over the CONUS between March–May of 2020 and 2019. The table also shows the correlation coefficient of all parameters with $PM_{2.5}$ in 2019 ($R2019$) and 2020 ($R2020$). The units for the parameters are as follows: T (k), Hum (10^{-3} kg/kg), Pres (millibars), PBL (m), Dust (10^{-11} kg/m³), Salt (10^{-11} kg/m³), BC (10^{-11} kg/m³), OC (10^{-11} kg/m³), SO_2 (10^{-11} kg/m³), SO_4 (10^{-11} kg/m³), NO_2 (ppb), and $PM_{2.5}$ (µg/m³).

		T	Hum	Pres	PBLH	Dust	Salt	BC	OC	SO₂	SO₄	NO₂	PM₂.₅
Washington DC	**R2019**	0.07	0.16	0.20	−0.36	0.10	−0.16	0.45	0.37	0.38	0.31	0.42	–
	R2020	0.13	0.12	0.21	−0.16	0.25	−0.14	0.50	0.32	0.49	0.00	0.63	–
	Diff.	−1.56	−1	−9.31	64.00	20.9	36	−8.53	−64.5	−4.51	−0.57	2.42	−1.37
	%	−0.55	−14.7	−0.01	8.05	14.62	22.22	−8.81	−17.4	−7.70	−0.17	−23.6	−21.1
New York	**R2019**	−0.08	0.06	0.18	−0.37	0.02	−0.01	0.57	0.40	0.53	0.32	0.64	–
	R2020	0.13	0.17	0.12	−0.45	−0.04	0.00	0.65	0.68	0.51	0.11	0.70	–
	Diff.	−0.65	−0.7	−63.6	87.9	22.4	39.3	−8.3	−45.9	−52.9	−29.4	−3.62	−1.52
	%	−0.23	−10.2	−0.06	12.53	17.54	17.87	−7.69	−13.7	−5.36	−7.94	−26.6	−20.7
Boston	**R2019**	−0.35	−0.25	0.41	−0.19	−0.07	−0.14	0.64	0.36	0.71	0.09	0.70	–
	R2020	0.06	0.05	0.18	−0.37	−0.05	0.04	0.59	0.54	0.67	0.23	0.51	–
	Diff.	0.17	−0.4	−89	50.3	22.4	104	−4.50	−6.69	13.5	−23.2	−2.57	−1.18
	%	0.06	−7.33	−0.09	7.04	21.80	42.22	−6.24	−2.82	3.37	−8.34	−28.1	−18.5
Los Angeles	**R2019**	0.75	0.14	0.00	−0.26	0.27	0.01	0.71	0.75	0.59	0.29	0.44	–
	R2020	0.81	0.11	−0.13	−0.61	0.44	0.42	0.78	0.62	0.62	0.12	0.39	–
	Diff.	0.84	−0.1	42.2	−4.27	32.8	26.2	2.4	22.3	−13.7	−29.8	−1.54	−0.22
	%	0.29	−1.99	0.04	−0.61	19	16.95	3.76	9.70	−1.69	−11.4	−15.6	−3.29
Chicago	**R2019**	−0.14	−0.15	0.32	−0.22	0.17	−0.46	0.54	0.29	0.62	0.31	0.72	–
	R2020	0.02	0.03	−0.03	−0.38	−0.07	−0.35	0.63	0.45	0.56	0.48	0.60	–
	Diff.	0.24	0	20.70	44.60	6.22	17.3	−5.20	−66.9	−66.5	3.22	−2.37	−0.66
	%	0.09	−0.12	0.02	6.95	3.56	15.06	−5.94	−19.3	−8.42	0.87	−17.4	−8.05
Houston	**R2019**	0.27	0.30	−0.16	−0.02	0.11	0.47	0.20	0.24	0.18	0.09	0.00	–
	R2020	0.33	0.36	−0.32	−0.13	−0.28	0.30	0.30	0.31	−0.01	−0.10	0.10	–
	Diff.	1.73	0.2	−24.2	15.15	12.4	−1.51	2.30	23.6	−19.6	−13.5	−1.36	−0.34
	%	0.59	1.79	−0.02	2.12	8.31	−25.2	7.21	9.06	−2.95	−6.31	−18.7	−3.63
Philadelphia	**R2019**	−0.09	0.02	0.22	−0.23	0.02	−0.19	0.57	0.30	0.50	0.34	0.51	–
	R2020	0.13	0.13	0.10	−0.22	0.04	−0.05	0.47	0.57	0.44	0.07	0.66	–
	Diff.	−1.24	−0.9	−37.5	67.5	26.8	35	−14.8	−157	−70.8	−3.54	1.67	−0.33
	%	−0.44	−12.6	−0.04	8.48	20.1	21.23	−9.94	−31	−8.59	−1.04	−16	−4.82
Detroit	**R2019**	−0.13	−0.10	0.34	−0.21	0.09	−0.38	0.59	0.24	0.62	0.18	0.74	–
	R2020	0.02	0.05	0.06	−0.52	0.01	−0.29	0.75	0.59	0.65	0.47	0.69	–
	Diff.	−0.06	−0.1	12.7	60.2	−17.9	15	−4.30	−71.7	−19.4	−40.9	−3.1	−1.16
	%	−0.02	−2.4	0.01	8.87	−9.17	13.11	−6.48	−24	−2.39	−10.3	−24.1	−13.5
Phoenix	**R2019**	0.34	−0.04	0.23	−0.37	−0.11	−0.38	0.65	0.32	0.73	0.37	0.59	–
	R2020	0.81	−0.36	−0.25	0.15	0.28	0.07	0.38	0.70	0.00	0.09	0.39	–
	Diff.	1.06	0.1	103	−19.2	−29.7	24.8	5.88	22.6	7.57	14.2	1.73	0.28
	%	0.36	2.17	0.11	−1.50	−4.28	33.43	10.52	13.06	3.72	11.39	−13.2	5.50
Dallas	**R2019**	0.00	−0.02	0.22	−0.14	−0.11	0.18	0.20	0.17	0.48	0.36	0.38	–
	R2020	0.27	0.24	−0.21	−0.13	−0.26	0.22	0.25	0.27	0.37	0.10	0.19	–
	Diff.	1.42	0	4.35	−20.2	20.1	−37.2	−0.7	−40.8	−6.64	−6.47	−0.68	−0.54
	%	0.49	0.75	0.00	−2.76	11.03	−20	−1.48	−11.5	−1.82	−2.56	−11.6	−6.71
Seattle	**R2019**	0.17	0.13	0.17	−0.18	0.25	−0.29	0.35	0.47	0.56	−0.17	0.56	–
	R2020	−0.11	−0.24	0.16	−0.41	0.23	−0.22	0.52	0.52	0.81	−0.07	0.69	–
	Diff.	−1.05	−0.4	81.1	77.2	3.07	8.09	−3.44	−39.2	−9.68	−1.65	3.42	−0.42
	%	−0.37	−6.9	0.08	12.10	3.11	5.99	−5.15	−16	−3.97	−1.08	−24.3	−7.73

the true linear regression line of the total population lies. The CI shows the uncertainty of the relationship between $PM_{2.5}$ percentage changes in March–May 2020 compared to 2019 and vehicular $PM_{2.5}$. However, a small significance F (almost 0.0058) of the linear regression in Fig. 4 indicates that the linear relationship between $PM_{2.5}$ percentage changes and vehicular $PM_{2.5}$ is significant.

4.4. Impact of meteorology and precursors on changes in $PM_{2.5}$

Table 4 shows the relationship between daily $PM_{2.5}$ changes and daily variations in several parameters, including air temperature, specific humidity, surface pressure, PBLH, and surface concentrations of dust, sea salt, BC, OC, SO_2, SO_4, and NO_2 between March–May of 2020 and 2019, in the eleven urban environments over the CONUS. The table lists the correlation coefficients of all parameters with $PM_{2.5}$ in 2019 and 2020 (henceforth referred to as $R2019$-$PM_{2.5}$ and $R2020$-$PM_{2.5}$, respectively) along with their absolute and percentage changes occurring between March–May of 2020 and 2019.

The results in Table 4 show that Washington DC experienced the highest reduction in $PM_{2.5}$ (−21.1%) in March–May of 2020 compared to 2019. The table shows no major changes in meteorological factors in

Washington DC between 2020 and 2019, except for air temperature ($R2020$-$PM_{2.5}$ = 0.13), which decreased by 1.56 K in 2020. There is usually a positive correlation between $PM_{2.5}$ and air temperature since an increase in temperature can promote the conversion of NO_2 and SO_2 to nitrate and sulfate (Lin et al., 2019; Ghahremanloo et al., 2021b), respectively, increasing $PM_{2.5}$ levels. Increased temperature can also result in more biogenic emissions, which, in turn, leads to more $PM_{2.5}$ concentrations (Di et al., 2016; Ghahremanloo et al., 2021b). It should be noted that elevated temperature can also promote air convection resulting in dispersion situations that reduce pollution levels (Luo et al., 2017; Pouyaei et al., 2021; Yang et al., 2017). The relationship between $PM_{2.5}$ and temperature ($R2020$-$PM_{2.5}$ = 0.13) in Washington DC, however, was weak, indicating that the temperature was unlikely to have impacted $PM_{2.5}$ levels in this region in 2020. $PM_{2.5}$ is more strongly associated with other parameters, particularly surface NO_2 concentrations ($R2020$-$PM_{2.5}$ = 0.63), with a 2.42 ppb (−23.64%) decrease in 2020 compared to 2019 in Washington DC. $PM_{2.5}$ concentrations also show a moderate correlation with BC ($R2020$-$PM_{2.5}$ = 0.50), OC ($R2020$-$PM_{2.5}$ = 0.32), and SO_2 ($R2020$-$PM_{2.5}$ = 0.49), with a decrease of 8.81%, 17.40%, and 7.7%, respectively, in 2020 compared to 2019. In fact, as BC, OC, and SO_4 make up a portion of $PM_{2.5}$, any changes they

undergo directly influence PM$_{2.5}$ concentrations (Bell et al., 2007; Ghahremanloo et al., 2021b). SO$_2$ and NO$_2$ are also precursors of sulfate and nitrate, which comprise a large portion of PM$_{2.5}$. Therefore, as vehicular emissions are main source of NO$_2$, SO$_2$, SO$_4$, OC, and BC concentrations in the atmosphere (Cao et al., 2006; Ghahremanloo et al., 2021b; Ni et al., 2014; Yang et al., 2018), a decrease in vehicular use and emissions, especially in Washington DC, with relatively high levels of vehicular PM$_{2.5}$, can lead to reduced PM$_{2.5}$ levels, as shown in Section 4.3.

In New York, PM$_{2.5}$ concentrations decreased by 20.7% between March–May of 2020 and 2019. Table 3 shows that one of the greatest reductions in human mobility to various categories of places occurred in New York. Table 4 shows that PM$_{2.5}$ levels in New York are strongly associated with NO$_2$ concentrations ($R2020$-PM$_{2.5}$ = 0.70), which decreased by 26.6% in 2020 compared to 2019, indicating that the decrease in NO$_2$ was main reason for the decrease in PM$_{2.5}$ levels in this region. In addition, PM$_{2.5}$ reduction in New York could have partly been due to small decreases in concentrations of BC ($R2020$-PM$_{2.5}$ = 0.65), OC ($R2020$-PM$_{2.5}$ = 0.68), and SO$_2$ ($R2020$-PM$_{2.5}$ = 0.51) resulting from the relatively strong correlations between these pollutants and PM$_{2.5}$. In addition, New York saw an increase of 87.9 m (12.53%) in the PBLH ($R2020$-PM$_{2.5}$ = −0.45) during March–May 2020 compared to 2019. Since pollutants are distributed throughout a higher volume of air, an elevated PBLH can reduce air pollution levels (Su et al., 2018). Thus, the PBLH could have been partially responsible for the PM$_{2.5}$ reduction in New York. A 7.04% increase in the PBLH ($R2020$-PM$_{2.5}$ = −0.37) may also have been partially responsible for the PM$_{2.5}$ reduction (−18.5%) in Boston in 2020. Most of the reduction in PM$_{2.5}$, however, can be attributed to decreased concentrations of BC (−6.24%; $R2020$-PM$_{2.5}$ = 0.59), OC (−2.82%; $R2020$-PM$_{2.5}$ = 0.54), sulfate (−8.34%; $R2020$-PM$_{2.5}$ = 0.23), and particularly NO$_2$ (−28.1%; $R2020$-PM$_{2.5}$ = 0.51). It should be noted that Washington DC, New York, and Boston had the highest percentage decreases in the number of visitors to various categories of places and the highest percentage increases in the amount of time people stayed in their residential areas during March–May 2020 compared to baseline, resulting in large reductions in PM$_{2.5}$ levels. Compared to other regions in this study, these urban environments also had relatively high vehicular PM$_{2.5}$.

In Los Angeles, unlike in Washington DC, New York, and Boston, PM$_{2.5}$ levels only slightly declined (−3.29%) during March–May 2020 compared to 2019. Table 4 shows a 0.84 K increase in the temperature in Los Angeles between March–May of 2020 and 2019. The strong relationship between PM$_{2.5}$ and temperature in 2019 and 2020 ($R2019$-PM$_{2.5}$ = 0.75 and $R2020$-PM$_{2.5}$ = 0.81, respectively) indicates that temperature strongly impacted the PM$_{2.5}$ levels in Los Angeles, although temperature increase is not significant in 2020. Dust ($R2020$-PM$_{2.5}$ = 0.44), sea salt ($R2020$-PM$_{2.5}$ = 0.42), BC ($R2020$-PM$_{2.5}$ = 0.78), and OC ($R2020$-PM$_{2.5}$ = 0.62) also increased by 19%, 16.95%, 3.76%, and 9.70%, respectively, while SO$_4$ ($R2020$-PM$_{2.5}$ = 0.12) and NO$_2$ ($R2020$-PM$_{2.5}$ = 0.39) decreased by 11.4% and 15.6%, respectively, in Los Angeles between 2020 and 2019. Because of their moderate to high correlation with PM$_{2.5}$ changes, the increases in the levels of temperature, dust, sea salt, BC, and OC could, to some extent, have been responsible for the slight reduction of PM$_{2.5}$ in Los Angeles. Results show that in Chicago, BC ($R2020$-PM$_{2.5}$ = 0.63), OC ($R2020$-PM$_{2.5}$ = 0.45), SO$_2$ ($R2020$-PM$_{2.5}$ = 0.56), and NO$_2$ ($R2020$-PM$_{2.5}$ = 0.60) decreased by 5.94%, 19.3%, 8.42%, and 17.4%, respectively, between 2020 and 2019, reducing PM$_{2.5}$ levels by 8.05% between the two years.

Table 4 shows only 3.63% decrease in PM$_{2.5}$ levels in Houston during the study period in 2020 compared to 2019. A 1.73 K increase in temperature ($R2020$-PM$_{2.5}$ = 0.33) between 2020 and 2019 could have contributed to the slight increase in PM$_{2.5}$ levels in Houston. Despite the increase in the levels of BC (7.21%; $R2020$-PM$_{2.5}$ = 0.30) and OC (9.6%; $R2020$-PM$_{2.5}$ = 0.31) in Houston, SO$_2$, SO$_4$, and NO$_2$ decreased by 2.95%, 6.31%, and 18.7%, respectively, during the study period. The results, however, show no relationship between PM$_{2.5}$ levels and

concentrations of SO$_2$ ($R2020$-PM$_{2.5}$ = −0.01), SO$_4$ ($R2020$-PM$_{2.5}$ = −0.1), and NO$_2$ ($R2020$-PM$_{2.5}$ = −0.1) in Houston in 2020. Accordingly, Fig. 4 and Table 3 also show relatively low vehicular PM$_{2.5}$ in Houston, compared to other urban environments, along with relatively small changes in the number of visitors to various categories of places. Houston experienced the lowest percentage reduction in the number of people visiting grocery stores and pharmacies (−1.49%) (Table 3) and one of the lowest percentage reductions in other categories, explaining the relatively small reduction in PM$_{2.5}$ levels in March–May 2020 compared to 2019. Moreover, the increase in the amount of time people stayed at their residential areas in Houston was relatively small compared to other regions. Philadelphia also experienced a 4.82% decrease in PM$_{2.5}$ concentrations between 2020 and 2019, possibly influenced by decreases in BC (−9.94%; $R2020$-PM$_{2.5}$ = 0.47), SO$_2$ (8.59%; $R2020$-PM$_{2.5}$ = 0.44), and especially OC (−31%; $R2020$-PM$_{2.5}$ = 0.57) and NO$_2$ (−16%; $R2020$-PM$_{2.5}$ = 0.66). In Detroit, a 13.5% decrease in PM$_{2.5}$ concentrations between March–May of 2020 and 2019 can also be attributed to decreases in the concentrations of BC (−6.48%; $R2020$-PM$_{2.5}$ = 0.75), OC (−24%; $R2020$-PM$_{2.5}$ = 0.59), SO$_2$ (−2.39%; $R2020$-PM$_{2.5}$ = 0.65), SO$_4$ (−10.3%; $R2020$-PM$_{2.5}$ = 0.47), and NO$_2$ (−24.1%; $R2020$-PM$_{2.5}$ = 0.69). In addition, an 8.87% increase in the PBLH ($R2020$-PM$_{2.5}$ = −0.52) in 2020 may have led to decreases in the PM$_{2.5}$ levels in Detroit.

Phoenix is the only region in this study that experienced an increase (5.5%) in PM$_{2.5}$ levels during March–May 2020 compared to similar days in 2019. Table 4 shows that the concentrations of BC ($R2020$-PM$_{2.5}$ = 0.38), OC ($R2020$-PM$_{2.5}$ = 0.70), SO$_2$ ($R2020$-PM$_{2.5}$ = 0.0), and SO$_4$ ($R2020$-PM$_{2.5}$ = 0.09) increased by 10.52%, 13.06%, 3.72%, and 11.39%, respectively, between 2020 and 2019. Although the results show no relationship between PM$_{2.5}$ and concentrations of SO$_2$ and SO$_4$, the correlation of PM$_{2.5}$ with BC and especially OC in 2020 appears to be strong. Furthermore, the significant correlation between PM$_{2.5}$ and temperature in 2020, along with a 1.06 K increase in temperature, could have increased PM$_{2.5}$ concentrations in this region. It should be noted that NO$_2$ levels decreased by 13.2% ($R2020$-PM$_{2.5}$ = 0.39) in Phoenix between 2020 and 2019 and that Phoenix had the lowest rate of vehicular PM$_{2.5}$ emissions (Fig. 4) than the other urban regions in this study. The city also had some of the lowest reductions in human mobility in the "Grocery-Pharmacy" (−7%), "Workplace" (−34.13%, the lowest reduction), and "Transit Stations" (−31.16%) categories. In addition, Phoenix showed the lowest percentage increase in the amount of time people stayed in their residential areas, further highlighting the relatively poor application and enforcement of stay-at-home strategies in this region, which potentially limited the reduction of PM$_{2.5}$ in Phoenix.

The results showed a decrease of 6.71% in PM$_{2.5}$ levels in Dallas in March–May 2020 compared to previous year and a decrease of 20%, 1.48%, 11.5%, 1.82%, 2.56%, and 11.6% in the concentrations of sea salt ($R2020$-PM$_{2.5}$ = 0.22), BC ($R2020$-PM$_{2.5}$ = 0.25), OC ($R2020$-PM$_{2.5}$ = 0.27), SO$_2$ ($R2020$-PM$_{2.5}$ = 0.37), SO$_4$ ($R2020$-PM$_{2.5}$ = 0.10), and NO$_2$ ($R2020$-PM$_{2.5}$ = 0.19), respectively, in Dallas between March–May of 2020 and 2019. However, the 1.42 K increase in temperature, with a relatively low correlation with PM$_{2.5}$ ($R2020$-PM$_{2.5}$ = 0.27) in 2020, could have contributed to the slight increase in PM$_{2.5}$ in this urban area. The results listed in Table 3 also reveal that reductions in mobility in Dallas were not as significant as they were in other areas, and people spent relatively less time in residential areas in Dallas than they did in other regions. In Seattle, PM$_{2.5}$ levels decreased by 7.73% during March–May 2020 compared to similar days in 2019. Table 4 lists a 5.15%, 16%, 3.97%, 1.08%, and 24.3% reductions in the concentrations of BC ($R2020$-PM$_{2.5}$ = 0.52), OC ($R2020$-PM$_{2.5}$ = 0.52), SO$_2$ ($R2020$-PM$_{2.5}$ = 0.81), SO$_4$ ($R2020$-PM$_{2.5}$ = −0.07), and NO$_2$ ($R2020$-PM$_{2.5}$ = 0.69) in Seattle between March–May of 2020 and 2019. Decreases in the concentrations of BC, OC, SO$_2$, and NO$_2$, along with their strong relationship to PM$_{2.5}$, could explain the 7.73% decrease in PM$_{2.5}$ concentrations in Seattle between March–May 2020 and the previous year. In addition, an increase in the PBLH ($R2020$-PM$_{2.5}$ = −0.41) of 12.1%

between 2020 and 2019 could have been partially responsible for the reduction of $PM_{2.5}$ in 2020.

5. Conclusion

The main purpose of this study was to examine the impact of the COVID-19 outbreak on $PM_{2.5}$ levels in eleven urban environments (Washington DC, New York, Boston, Chicago, Los Angeles, Houston, Dallas, Philadelphia, Detroit, Phoenix, and Seattle) across the United States. We used a Deep-CNN to accurately capture the spatiotemporal distribution of $PM_{2.5}$ levels at a 5-km spatial resolution over the CONUS in March–May 2019 and 2020. The Deep-CNN model showed promising accuracy at $PM_{2.5}$ estimation, with an R, IOA, MAE, and RMSE of 0.90 (0.90), 0.95 (0.95), 1.34 (1.24) $\mu g/m^3$, and 2.04 (1.87) $\mu g/m^3$, respectively, in March–May 2019 (2020). Results of the Google Community Mobility Reports and the estimated $PM_{2.5}$ levels revealed a high correlation between changes in human mobility and $PM_{2.5}$ concentrations, indicating that regions with more reductions in human mobility also experienced more reductions in $PM_{2.5}$ levels. The correlation coefficient between $PM_{2.5}$ percentage changes in all regions and corresponding percentage changes in the number of visitors to "grocery stores and pharmacies", "workplaces", and "transit stations" were 0.67, 0.83, and 0.61, respectively. Moreover, percentage changes in $PM_{2.5}$ and the amount of time people stayed in their residential areas during the pandemic were also strongly correlated ($R = -0.87$), indicating greater reductions in $PM_{2.5}$ levels in urban environments in which people stayed longer in their residential areas. The relatively strong correlation between vehicular $PM_{2.5}$ and percentage changes in $PM_{2.5}$ ($R = -0.77$) in study regions showed greater $PM_{2.5}$ reductions in regions with higher vehicular $PM_{2.5}$ emissions. Among the eleven urban environments, Washington DC, New York, and Boston experienced the greatest reductions in their mean $PM_{2.5}$ levels (i.e., -21.1%, -20.7%, and -18.5%, respectively) between March–May of 2020 and 2019. These same three urban environments also experienced greater reductions in human mobility and one of the highest vehicular $PM_{2.5}$ emissions compared to other regions in this study. All of the other urban environments (Los Angeles, Chicago, Houston, Dallas, Philadelphia, Detroit, and Seattle) experienced decreases in $PM_{2.5}$ levels by 3.29%, 8.05%, 3.63%, 6.71%, 4.82%, 13.5%, and 7.73%, respectively, in 2020 compared to 2019. An exception, however, is Phoenix, with a 5.5% increase in $PM_{2.5}$ concentrations during the same period. According to the results, changes in the concentrations of pollutants, BC, OC, SO_2, SO_4, and especially NO_2, had a significantly higher impact on changes in $PM_{2.5}$ concentrations in 2020 than meteorological factors, although there was a strong relationship between air temperature and $PM_{2.5}$ levels in Los Angeles ($R2020\text{-}PM_{2.5} = 0.81$) and Phoenix ($R2020\text{-}PM_{2.5} = 0.81$). The increase in $PM_{2.5}$ levels (5.5%) in Phoenix could be attributed to increased levels of BC, OC, and air temperature and the relatively low rate of vehicular $PM_{2.5}$ emissions in this region. In addition, one of the lowest reductions in human mobility to various categories of places occurred in Phoenix, further explaining the increased $PM_{2.5}$ concentrations in this urban environment.

CRediT authorship contribution statement

Masoud Ghahremanloo: Conceptualization, Data curation, Formal analysis, Investigation, Methodology, Project administration, Software, Validation, Visualization, Writing – original draft, Writing – review & editing. **Yannic Lops:** Data curation, Formal analysis, Software, Writing – review & editing. **Yunsoo Choi:** Conceptualization, Funding acquisition, Methodology, Supervision, Writing – review & editing. **Jia Jung:** Data curation, Writing – original draft, Writing – review & editing. **Seyedali Mousavinezhad:** Data curation, Writing – review & editing. **Davyda Hammond:** Funding acquisition, Writing – review & editing.

Declaration of competing interest

The authors declare that they have no known competing financial interests or personal relationships that could have appeared to influence the work reported in this paper.

Appendix A. Supplementary data

Supplementary data to this article can be found online at https://doi.org/10.1016/j.atmosenv.2022.118944.

References

Adams-Prassl, A., Boneva, T., Golin, M., Rauh, C., 2020. The Impact of the Coronavirus Lockdown on Mental Health: Evidence from the US.

Aubrey, A., January 31, 2020. Trump Declares Coronavirus A Public Health Emergency and Restricts Travel from China. NPR. Retrieved March 18, 2020, from. https://www.npr.org/sections/health-shots/2020/01/31/801686524/trump-declares-coronavirus-a-public-health-emergency-and-restricts-travel-from-c.

Baldasano, J.M., 2020. COVID-19 lockdown effects on air quality by NO2 in the cities of Barcelona and Madrid (Spain). Sci. Total Environ. 741, 140353.

Banks, J., Xu, X., 2020. The Mental Health Effects of the First Two Months of Lockdown and Social Distancing during the Covid-19 Pandemic in the UK (No. W20/16). IFS Working Papers.

Bao, R., Zhang, A., 2020. Does lockdown reduce air pollution? Evidence from 44 cities in northern China. Sci. Total Environ. 731, 139052.

Bedimo-Rung, A.L., Mowen, A.J., Cohen, D.A., 2005. The significance of parks to physical activity and public health: a conceptual model. Am. J. Prev. Med. 28 (2), 159–168.

Bell, M.L., Dominici, F., Ebisu, K., Zeger, S.L., Samet, J.M., 2007. Spatial and temporal variation in PM2.5 chemical composition in the United States for health effects studies. Environ. Health Perspect. 115 (7), 989–995.

Bherwani, H., Gupta, A., Anjum, S., Anshul, A., Kumar, R., 2020. Exploring dependence of COVID-19 on environmental factors and spread prediction in India. NPJ Clim. Atmos. Sci. 3 (1), 1–13.

Bouarar, I., Gaubert, B., Brasseur, G.P., Steinbrecht, W., Doumbia, T., Tilmes, S., et al., 2021. Ozone anomalies in the free troposphere during the COVID-19 pandemic. Geophys. Res. Lett. 48 (16), e2021GL094204.

Cao, G., Zhang, X., Zheng, F., 2006. Inventory of black carbon and organic carbon emissions from China. Atmos. Environ. 40 (34), 6516–6527.

Cascella, M., Rajnik, M., Aleem, A., Dulebohn, S., Di Napoli, R., 2021. Features, Evaluation, and Treatment of Coronavirus (COVID-19). StatPearls.

Cenfetelli, R.T., Bassellier, G., 2009. Interpretation of formative measurement in information systems research. MIS Q. 689–707.

Chauhan, A., Singh, R.P., 2020. Decline in PM2.5 concentrations over major cities around the world associated with COVID-19. Environ. Res. 187, 109634.

Chen, K.L., Henneman, L.R., Nethery, R.C., 2021. Differential Impacts of COVID-19 Lockdowns on PM2. 5 across the United States. medRxiv.

Chow, J.C., Watson, J.G., Green, M.C., Lowenthal, D.H., Bates, B., Oslund, W., Torres, G., 2000. Cross-border transport and spatial variability of suspended particles in Mexicali and California's Imperial Valley. Atmos. Environ. 34 (11), 1833–1843.

de Hoogh, K., Saucy, A., Shtein, A., Schwartz, J., West, E.A., Strassmann, A., et al., 2019. Predicting fine-scale daily NO2 for 2005–2016 incorporating OMI satellite data across Switzerland. Environ. Sci. Technol. 53 (17), 10279–10287.

Di, Q., Kloog, I., Koutrakis, P., Lyapustin, A., Wang, Y., Schwartz, J., 2016. Assessing PM2.5 exposures with high spatiotemporal resolution across the continental United States. Environ. Sci. Technol. 50 (9), 4712–4721.

Elmer, T., Mepham, K., Stadtfeld, C., 2020. Students under lockdown: comparisons of students' social networks and mental health before and during the COVID-19 crisis in Switzerland. PLoS One 15 (7), e0236337.

Eslami, E., Choi, Y., Lops, Y., Sayeed, A., 2020. A real-time hourly ozone prediction system using deep convolutional neural network. Neural Comput. Appl. 32 (13), 8783–8797.

García, M.V., Aznarte, J.L., 2020. Shapley additive explanations for NO2 forecasting. Ecol. Inf. 56, 101039.

Gautam, S., 2020. COVID-19: air pollution remains low as people stay at home. Air Qual. Atmos. Health 13, 853–857.

Ghahremanloo, M., Choi, Y., Sayeed, A., Salman, A.K., Pan, S., Amani, M., 2021b. Estimating daily high-resolution PM2.5 concentrations over Texas: machine Learning approach. Atmos. Environ. 247, 118209.

Ghahremanloo, M., Lops, Y., Choi, Y., Mousavinezhad, S., 2021a. Impact of the COVID-19 outbreak on air pollution levels in East Asia. Sci. Total Environ. 754, 142226.

Ghahremanloo, M., Lops, Y., Choi, Y., Yeganeh, B., 2021c. Deep learning estimation of daily ground level NO2 concentrations from remote sensing data. J. Geophys. Res. Atmos. 126, e2021JD034925 https://doi.org/10.1029/2021JD034925.

Hasheminassab, S., Daher, N., Ostro, B.D., Sioutas, C., 2014. Long-term source apportionment of ambient fine particulate matter (PM2. 5) in the Los Angeles Basin: a focus on emissions reduction from vehicular sources. Environ. Pollut. 193, 54–64.

Hayes, R.B., Lim, C., Zhang, Y., Cromar, K., Shao, Y., Reynolds, H.R., et al., 2020. PM2.5 air pollution and cause-specific cardiovascular disease mortality. Int. J. Epidemiol. 49 (1), 25–35.

Hu, X., Belle, J.H., Meng, X., Wildani, A., Waller, L.A., Strickland, M.J., Liu, Y., 2017. Estimating PM2.5 concentrations in the conterminous United States using the random forest approach. Environ. Sci. Technol. 51 (12), 6936–6944.

Hu, X., Waller, L.A., Lyapustin, A., Wang, Y., Al-Hamdan, M.Z., Crosson, W.L., et al., 2014. Estimating ground-level PM2.5 concentrations in the Southeastern United States using MAIAC AOD retrievals and a two-stage model. Rem. Sens. Environ. 140, 220–232.

Huang, S., Song, S., Nielsen, C.P., Zhang, Y., Xiong, J., Weschler, L.B., et al., 2022. Residential building materials: an important source of ambient formaldehyde in mainland China. Environ. Int. 158, 106909.

Jaffe, D., Bertschi, I., Jaeglé, L., Novelli, P., Reid, J.S., Tanimoto, H., et al., 2004. Long-range transport of Siberian biomass burning emissions and impact on surface ozone in western North America. Geophys. Res. Lett. 31 (16).

Karnae, S., John, K., 2019. Source apportionment of PM2. 5 measured in South Texas near USA–Mexico border. Atmos. Pollut. Res. 10 (5), 1663–1676.

Khan, I., Shah, D., Shah, S.S., 2021. COVID-19 pandemic and its positive impacts on environment: an updated review. Int. J. Environ. Sci. Technol. 18 (2), 521–530.

Kline, R.B., 2015. Principles and Practice of Structural Equation Modeling. Guilford publications.

Kock, N., Lynn, G., 2012. Lateral collinearity and misleading results in variance-based SEM: an illustration and recommendations. J. Assoc. Inf. Syst. Online 13 (7).

Krecl, P., Targino, A.C., Oukawa, G.Y.C., Junior, R.P.C., 2020. Drop in urban air pollution from COVID-19 pandemic: policy implications for the megacity of São Paulo. Environ. Pollut. 265 (114883) https://doi.org/10.1016/j.envpol.2020.114883.

Kroll, C.N., Song, P., 2013. Impact of multicollinearity on small sample hydrologic regression models. Water Resour. Res. 49 (6), 3756–3769.

Lal, P., Kumar, A., Kumar, S., Kumari, S., Saikia, P., Dayanandan, A., et al., 2020. The dark cloud with a silver lining: assessing the impact of the SARS COVID-19 pandemic on the global environment. Sci. Total Environ. 732, 139297.

Lancet, T., 2006. WHO's Global Air-Quality Guidelines.

Lee, H.J., Chatfield, R.B., Strawa, A.W., 2016. Enhancing the applicability of satellite remote sensing for PM2.5 estimation using MODIS deep blue AOD and land use regression in California, United States. Environ. Sci. Technol. 50 (12), 6546–6555.

Li, T., Shen, H., Yuan, Q., Zhang, X., Zhang, L., 2017. Estimating ground-level PM2.5 by fusing satellite and station observations: a geo-intelligent deep learning approach. Geophys. Res. Lett. 44 (23), 11–985.

Liang, Q., Jaeglé, L., Jaffe, D.A., Weiss-Penzias, P., Heckman, A., Snow, J.A., 2004. Long-range transport of Asian pollution to the northeast Pacific: seasonal variations and transport pathways of carbon monoxide. J. Geophys. Res. Atmos. 109 (D23).

Lin, C.A., Chen, Y.C., Liu, C.Y., Chen, W.T., Seinfeld, J.H., Chou, C.C.K., 2019. Satellite-derived correlation of SO2, NO2, and aerosol optical depth with meteorological conditions over East Asia from 2005 to 2015. Rem. Sens. 11 (15), 1738.

Liu, R., Ma, Z., Liu, Y., Shao, Y., Zhao, W., Bi, J., 2020. Spatiotemporal distributions of surface ozone levels in China from 2005 to 2017: a machine learning approach. Environ. Int. 142, 105823.

Lops, Y., Choi, Y., Eslami, E., Sayeed, A., 2020. Real-time 7-day forecast of pollen counts using a deep convolutional neural network. Neural Comput. Appl. 32 (15), 11827–11836.

Lops, Y., Pouyaei, A., Choi, Y., Jung, J., Salman, A.K., Sayeed, A., 2021. Application of a partial convolutional neural network for estimating geostationary aerosol optical depth data. Geophys. Res. Lett. 48 (15), e2021GL093096.

Lundberg, S.M., Lee, S.I., 2017. A unified approach to interpreting model predictions. In: Advances in Neural Information Processing Systems, pp. 4765–4774.

Luo, J., Du, P., Samat, A., Xia, J., Che, M., Xue, Z., 2017. Spatiotemporal pattern of PM2.5 concentrations in mainland China and analysis of its influencing factors using geographically weighted regression. Sci. Rep. 7 (1), 1–14.

Luo, L., Robock, A., Mitchell, K.E., Houser, P.R., Wood, E.F., Schaake, J.C., et al., 2003. Validation of the North American land data assimilation system (NLDAS) retrospective forcing over the southern Great Plains. J. Geophys. Res. Atmos. 108 (D22).

Mahato, S., Pal, S., Ghosh, K.G., 2020. Effect of lockdown amid COVID-19 pandemic on air quality of the megacity Delhi, India. Sci. Total Environ. 730, 139086.

Ni, M., Huang, J., Lu, S., Li, X., Yan, J., Cen, K., 2014. A review on black carbon emissions, worldwide and in China. Chemosphere 107, 83–93.

Otmani, A., Benchrif, A., Tahri, M., Bounakhla, M., El Bouch, M., Krombi, M.H., 2020. Impact of covid-19 lockdown on PM10, SO2 and NO2 concentrations in Salé city (Morocco). Sci. Total Environ. 735, 139541.

Pan, S., Jung, J., Li, Z., Hou, X., Roy, A., Choi, Y., Gao, H.O., 2020. Air quality implications of COVID-19 in California. Sustainability 12 (17), 7067.

Parida, B.R., Bar, S., Roberts, G., Mandal, S.P., Pandey, A.C., Kumar, M., Dash, J., 2021. Improvement in air quality and its impact on land surface temperature in major urban areas across India during the first lockdown of the pandemic. Environ. Res. 199, 111280.

Park, Y., Kwon, B., Heo, J., Hu, X., Liu, Y., Moon, T., 2020. Estimating PM2.5 concentration of the conterminous United States via interpretable convolutional neural networks. Environ. Pollut. 256, 113395.

Polezer, G., Tadano, Y.S., Siqueira, H.V., Godoi, A.F., Yamamoto, C.I., de André, P.A., et al., 2018. Assessing the impact of PM2. 5 on respiratory disease using artificial neural networks. Environ. Pollut. 235, 394–403.

Pouyaei, A., Choi, Y., Jung, J., Sadeghi, B., Song, C.H., 2020. Concentration trajectory route of air pollution with an integrated Lagrangian model (C-trail model v1. 0) derived from the community Multiscale Air quality model (CMAQ model v5. 2). Geosci. Model Dev. (GMD) 13 (8), 3489–3505.

Pouyaei, A., Sadeghi, B., Choi, Y., Jung, J., Souri, A.H., Zhao, C., Song, C.H., 2021. Development and implementation of a physics-based convective mixing scheme in the community Multiscale Air quality modeling framework. J. Adv. Model. Earth Syst. 13 (6), e2021MS002475.

Robertson, L., April 15, 2020. Trump's Snowballing China Travel Claim. FactCheck.org. Retrieved April 29, 2020 from. https://www.factcheck.org/2020/04/trumps-snowballing-china-travel-claim/.

Rodríguez-Urrego, D., Rodríguez-Urrego, L., 2020. Air quality during the COVID-19: PM2.5 analysis in the 50 most polluted capital cities in the world. Environ. Pollut., 115042

Rossi, R., Socci, V., Talevi, D., Mensi, S., Niolu, C., Pacitti, F., et al., 2020. COVID-19 pandemic and lockdown measures impact on mental health among the general population in Italy. Front. Psychiatr. 11, 790.

Sayeed, A., Choi, Y., Eslami, E., Lops, Y., Roy, A., Jung, J., 2020. Using a deep convolutional neural network to predict 2017 ozone concentrations, 24 hours in advance. Neural Network. 121, 396–408.

Shap, 2019. Lundberg. https://github.com/slundberg/shap.

Su, T., Li, Z., Kahn, R., 2018. Relationships between the planetary boundary layer height and surface pollutants derived from lidar observations over China: regional pattern and influencing factors. Atmos. Chem. Phys. 18 (21), 15921–15935.

Tahir, M.B., Batool, A., 2020. COVID-19: healthy environmental impact for public safety and menaces oil market. Sci. Total Environ. 740, 140054.

Targino, A.C., Gibson, M.D., Krecl, P., Rodrigues, M.V.C., Dos Santos, M.M., de Paula Corrêa, M., 2016. Hotspots of black carbon and PM2. 5 in an urban area and relationships to traffic characteristics. Environ. Pollut. 218, 475–486.

Text, 1993-1994. - H.R.3450 - 103rd Congress. North American Free Trade Agreement Implementation Act. (1993, December 8). https://www.congress.gov/bill/103rd-congress/house-bill/3450/text.

Tobías, A., Carnerero, C., Reche, C., Massagué, J., Via, M., Minguillón, M.C., et al., 2020. Changes in air quality during the lockdown in Barcelona (Spain) one month into the SARS-CoV-2 epidemic. Sci. Total Environ. 726, 138540.

Tosepu, R., Gunawan, J., Effendy, D.S., Lestari, H., Bahar, H., Asfian, P., 2020. Correlation between weather and covid-19 pandemic in Jakarta, Indonesia. Sci. Total Environ. 725, 138436.

Viidanoja, J., Sillanpää, M., Laakia, J., Kerminen, V.M., Hillamo, R., Aarnio, P., Koskentalo, T., 2002. Organic and black carbon in PM2. 5 and PM10: 1 year of data from an urban site in Helsinki, Finland. Atmos. Environ. 36 (19), 3183–3193.

Wei, J., Huang, W., Li, Z., Xue, W., Peng, Y., Sun, L., Cribb, M., 2019. Estimating 1-km-resolution PM2.5 concentrations across China using the space-time random forest approach. Rem. Sens. Environ. 231, 111221.

WHO (World Health Organization), 2020. Coronavirus Disease 2019 (COVID-19) Situation Report-36. Available from:. World Health Organization Geneva. February 25, 2020. https://www.who.int/docs/default-source/coronaviruse/situation-reports/20200225-sitrep-36-covid-19.pdf.

Wood, L., Hooper, P., Foster, S., Bull, F., 2017. Public green spaces and positive mental health–investigating the relationship between access, quantity and types of parks and mental wellbeing. Health Place 48, 63–71.

Wu, J., Smith, S., Khurana, M., Siemaszko, C., DeJesus-Banos, B., 2020. Coronavirus Lockdowns and Stay-At-Home Orders across the U.S. Retrieved March 25, 2020, from. https://www.nbcnews.com/health/health-news/here-are-stay-home-orders-across-country-n1168736.

Xu, K., Cui, K., Young, L.H., Hsieh, Y.K., Wang, Y.F., Zhang, J., Wan, S., 2020. Impact of the COVID-19 event on air quality in central China. Aerosol Air Qual. Res. 20 (5), 915–929.

Yang, M., Ma, T., Sun, C., 2018. Evaluating the impact of urban traffic investment on SO2 emissions in China cities. Energy Pol. 113, 20–27.

Yang, Q., Yuan, Q., Li, T., Shen, H., Zhang, L., 2017. The relationships between PM2.5 and meteorological factors in China: seasonal and regional variations. Int. J. Environ. Res. Publ. Health 14 (12), 1510.

Yeo, I., Choi, Y., Lops, Y., Sayeed, A., 2021. Efficient PM2.5 forecasting using geographical correlation based on integrated deep learning algorithms. Neural Comput. Appl. 1–17.

Yin, H., Liu, C., Hu, Q., Liu, T., Wang, S., Gao, M., et al., 2021. Opposite impact of emission reduction during the COVID-19 lockdown period on the surface concentrations of PM2. 5 and O3 in Wuhan, China. Environ. Pollut. 289, 117899.

Zangari, S., Hill, D.T., Charette, A.T., Mirowsky, J.E., 2020. Air quality changes in New York City during the COVID-19 pandemic. Sci. Total Environ. 742, 140496.